Fast numerical 3D-Scheme for the Simulation of Hysteresis in ferromagnetic Materials

Ben Van de Wiele, Luc Dupré, *Member, IEEE,* and Femke Olyslager, *Fellow, IEEE*

***Abstract*— The paper deals with a two-level model for the evaluation of the electromagnetic hysteresis behavior of ferromagnetic materials when applying a magnetic field. The model can be used to determine which mechanisms minimize material losses in electrical steels. The material is seen in a high-level part as an ensemble of interacting monocrystals, where each monocrystal is described in a low-level 3D micromagnetic model. In this paper the 3D micromagnetic model is presented in order to find which mechanisms influence the magnetization loops of monocrystals. The micromagnetic model is based on several interactions between the magnetization vectors M of elementary dipoles in the crystal and the applied field. These interactions contribute to the effective field, composed of the applied field, the exchange field, the anisotropy field, the magnetostatic field and the magneto-elastic field. The time variation of the magnetization vector M in each space point obeys the Landau-Lifshitz equation. Macroscopic magnetization loops are reconstructed considering the average magnetization in the direction of the applied field. The influence of crystal defects on the magnetization is included by means of the stress they induce in the lattice.**

***Index Terms*— crystal defects, hysteresis, Landau-Lifshitz, magnetization loop, micromagnetism, monocrystal**

I. INTRODUCTION

TO improve the performance of electromagnetic devices, like electrical machines and transformers, the overall losses in general and the iron losses in particular must be minimized. Classically, electrical steel is characterized and qualified by means of standards which are based on simple, unidirectional sinusoidal flux excitations using e.g. Epstein, ring core or single sheet measurement equipment. Generally, the measured iron losses in electromagnetic devices exceed the value based on these standard measurements (unidirectional sinusoidal excitation). This is caused by distorted flux distributions, local rotational excitations, short-circuit between neighboring laminations, changes in the magnetic characteristics due to the mechanical treatment, etc. Therefore, a profound study of the material behavior of electrical steel under application conditions is very important. This study is important for the producers of electrical steel as for the machine constructors, both aiming to maximize machine performances. Understanding the phenomena inside the machine core is an indispensable step in the process of developing electromagnetic devices with a higher efficiency, thus lower core losses, resulting in a lower energy consumption. Hence producers of electrical steels are not only interested in the material behavior under prescribed, strongly simplified conditions, but also under the realistic conditions in electromagnetic devices. Here, the relation between the electromagnetic behavior and the microstructure of the electrical steel is crucial as the microstructure is directly related to the material production and treatment techniques. Also machine constructors are interested in material behavior under application conditions with regard to the material choice when optimizing the design of the device. A good description of the magnetic behavior of ferromagnetic materials may start from microstructural features like the presence of lattice effects, grains, textures, stresses, crystal defects, etc. A physical material model becomes valuable when these microstructural features are translated into quantitative predictions about the magnetization dynamics. The establishment of the correlation between the macroscopic magnetic properties, such as the electromagnetic losses, and the microstructural features plays a crucial role in the adaption of material production technologies to improve the material quality

This work was supported by the Flemish government through the IWT PhD scholarship SB/51032.

B. Van de Wiele and L. dupré are with the Department of Electrical Energy, Systems and Automation, Ghent University, Sint-Pietersnieuwstraat 41, B-9000 Ghent, Belgium.

F. Olyslager is with the Department of Information Technology, Ghent University, Sint-Pietersnieuwstraat 41, B-9000 Ghent, Belgium.

II. MACROSCOPIC MAGNETIC MATERIAL MODEL

A ferromagnetic material can be magnetized when it is exposed to an external time varying magnetic field. However, there is no unique relation between the applied magnetic field and the magnetization of the crystal: no single valued magnetization curve is described, but instead a magnetization loop or hysteresis loop.

The macroscopic hysteresis loop characterizes the material losses when cyclic magnetic fields are applied. A two-level model helps us to understand which microstructural features can decrease the electromagnetic losses. In this model the macroscopic material is seen as an ensemble of N monocrystals, each described by a 3D-micromagnetic model (the lowest level). A macroscopic model (the highest level) describes the ensemble of monocrystals. Each monocrystal interacts with the magnetic field applied on the macroscopic material ($\mathbf{H}_{applied}$) on the one hand and the mean magnetizations $< \mathbf{M}_i >$ of all other monocrystals $i = 1..N$ on the other hand, together resulting in a space varying effective applied field $\mathbf{H}_{a,eff}(\mathbf{r})$. The link between the two models is the relation between the effective applied field felt by the monocrystal i, $\mathbf{H}_{a,eff}(\mathbf{r}_i)$ and the mean magnetization of the monocrystal $< \mathbf{M}_i >$.

$$\mathbf{H}_{a,eff}(\mathbf{r}_i) \leftrightarrow < \mathbf{M}_i > \tag{1}$$

In this paper the 3D-micromagnetic model describing the monocrystal is presented in order to find which mechanisms

influence the relation (1). The monocrystal is seen as an entity subjected to an effective applied field $\mathbf{H}_{a,eff}(\mathbf{r}_i)$, for the sake of clarity simply called the applied field $\mathbf{H}_a$.

The presented 3D-micromagnetic model is based on the Landau-Lifshitz-formalism [1], that describes the electromagnetic action at the level of magnetic dipoles, resulting in the damped precession movement of the local magnetization vector with constant amplitude. By means of the local (microscopic) effective field, the formalism allows us to account for both the magnetic short distance effects (e.g. exchange field, anisotropy field and magnetoelastic field) and the magnetic long distance effects (magnetostatic field, imposed magnetic field). The magnetoelastic field takes lattice defects into account via the stress they induce in the lattice.

Starting from a predefined microstructural state, the micromagnetic model must permit us to describe the mean magnetization $< \mathbf{M} >$ of the monocrystal in the form of magnetization loops, caused by a time varying magnetic field.

III. MICROMAGNETIC THEORY

The theory of ferromagnetic materials is based on the assumption, following Landau and Lifshitz [1], that the magnetization of magnetic dipoles $\mathbf{M}$ varies with the position, but that it has a fixed temperature dependent magnitude $|\mathbf{M}| = M_s$ (below Curie-temperature). In the theory, the Gibbs free energy (ϕ_G) represents the total energy density in the crystal. This energy density ϕ_G depends on the configuration of the magnetic dipoles $\mathbf{M} = M_s\mathbf{m}$ and is minimized in order to find equilibrium conditions for the magnetic dipoles [2], leading to the definition of the effective magnetic field ($\mathbf{H}_{eff}$) in each point of the crystal. The static micromagnetic equilibrium is expressed as

$$\mathbf{m}(\mathbf{r}) \times \mathbf{H}_{eff}(\mathbf{r}) = 0 \tag{2}$$

The effective field contains all influences of the total crystal on the magnetic dipole $\mathbf{M}$ at that place.

A. The effective field $\mathbf{H}_{eff}$

The effective field is composed of the applied field ($\mathbf{H}_a$), the exchange field ($\mathbf{H}_{exch}$), the anisotropy field ($\mathbf{H}_{ani}$), the magnetostatic field ($\mathbf{H}_{ms}$) and the magnetoelastic field ($\mathbf{H}_{me}$).

$$\mathbf{H}_{eff} = \mathbf{H}_a + \mathbf{H}_{exch} + \mathbf{H}_{ani} + \mathbf{H}_{ms} + \mathbf{H}_{me} \tag{3}$$

Here the exchange and anisotropy fields are (using the Einstein summation convention: when two equal indices are used, summation is made)

$$\mathbf{H}_{exch} = \frac{2A}{\mu_0 M_s}\nabla^2\gamma_i\mathbf{e}_i \tag{4}$$

$$\mathbf{H}_{ani} = -\frac{1}{\mu_0 M_s}\frac{\partial\phi_{ani}}{\partial\gamma_i}\mathbf{e}_i \tag{5}$$

with A the exchange stiffness and the anisotropy energy

$$\phi_{ani} = K_1(\alpha_1^2\alpha_2^2 + \alpha_2^2\alpha_3^2 + \alpha_3^2\alpha_1^2) + K_2\alpha_1^2\alpha_2^2\alpha_3^2 \tag{6}$$

where α_i is the direction cosine of the $\mathbf{m}$-vector with respect to the i^{th} crystallographic axis of the based centered cubic iron lattice, while γ_i refer to the direction cosines of $\mathbf{m}$ with respect to the (x,y,z)-coordinate system. K_1 and K_2 are anisotropy constants.

The magnetostatic field follows from $\nabla \cdot \mathbf{H}_{ms} = -\nabla \cdot \mathbf{M}$ and $\nabla \times \mathbf{H}_{ms} = 0$ using Greens functions:

$$\mathbf{H}_{ms} = \frac{M_s}{4\pi}\int_V \left(\frac{\mathbf{m}}{|\mathbf{r}-\mathbf{r}'|^3} - \frac{(\mathbf{m}\cdot(\mathbf{r}-\mathbf{r}'))(\mathbf{r}-\mathbf{r}')}{|\mathbf{r}-\mathbf{r}'|^5}\right)\mathrm{d}V' \tag{7}$$

Here is V the volume of the considered crystal.

The magnetoelastic field is given by

$$\mathbf{H}_{me} = -\frac{1}{\mu_0 M_s}\sigma_{ij}\frac{\partial}{\partial\gamma_k}\left(\epsilon_{kj}^Q(\boldsymbol{\alpha})\right)\mathbf{e}_i \tag{8}$$

where $\boldsymbol{\sigma}$ is the local stress tensor and $\boldsymbol{\epsilon}^Q$ is the free magnetostrain tensor with elements

$$\epsilon_{ij}^Q = \frac{3}{2}\lambda_{100}\left(\alpha_i\alpha_j - \frac{1}{3}\right)\delta_{ij} + \frac{3}{2}\lambda_{111}\alpha_i\alpha_j(1-\delta_{ij}) \tag{9}$$

with λ_{100} andλ_{111} magnetostriction constants while δ_{ij} is the kronecker symbol.

B. Crystal defects

As mentioned, the presence of crystal defects is taken into account by there characteristic stress distribution. In the model, edge dislocations, screw dislocations and point defects contribute to the total stress tensor $\boldsymbol{\sigma}$.

The non-zero components of the stress tensor $\boldsymbol{\sigma}^{edge}$ characteristic for an edge dislocation running through the origin, with dislocation axis parallel to the z-axis and Burgers vector $\mathbf{b}$ parallel with the x-axis are given by [3]

$$\sigma_{11}^{edge} = -\tau_0\frac{by(3x^2+y^2)}{(x^2+y^2)^2} \tag{10}$$

$$\sigma_{22}^{edge} = \tau_0\frac{by(x^2-y^2)}{(x^2+y^2)^2} \tag{11}$$

$$\sigma_{33}^{edge} = 2\tau_0\frac{\nu y}{x^2+y^2} \tag{12}$$

$$\sigma_{12}^{edge} = \sigma_{21}^{edge} = \tau_0\frac{bx(x^2-y^2)}{(x^2+y^2)^2} \tag{13}$$

with

$$\tau_0 = \frac{G}{2\pi(1-\nu)} \tag{14}$$

Here is b the length of the Burgers vector of the edge dislocation and G and ν the modulus of rigidity and Poisson's ratio respectively. In the monocrystal the Burgers vector is parallel with a $< 1\,1\,1 >$ direction, while the axis of the dislocation is parallel with a $< 1\,1\,0 >$ direction [4]. So the stress tensor $\boldsymbol{\sigma}^{edge}$ has to be transformed in terms of a proper rotation matrix $\mathbf{R}^{edge}$ to a stress tensor $\boldsymbol{\sigma}'^{edge}$ that incorporates the monocrystal by

$$\sigma_{ij}'^{edge} = R_{ik}^{edge}R_{jl}^{edge}\sigma_{kl}^{edge} \tag{15}$$

The non-zero components of the the stress tensor $\boldsymbol{\sigma}^{scr}$ characteristic for a screw dislocation running through the

origin and with dislocation axis parallel to the z-axis are given by [3]

$$\sigma_{13}^{scr} = \sigma_{31}^{scr} = -\frac{Gb}{2\pi}\frac{y}{x^2+y^2} \tag{16}$$

$$\sigma_{23}^{scr} = \sigma_{32}^{scr} = -\frac{Gb}{2\pi}\frac{x}{x^2+y^2} \tag{17}$$

For a screw dislocation the Burgers vector $\mathbf{b}$ is parallel with the axis of the dislocation and parallel with a $< 111 >$-direction. So the stress tensor $\boldsymbol{\sigma}^{scr}$ should also be transformed to $\boldsymbol{\sigma}'^{scr}$ to match the crystal lattice by a transformation similar to (15).

The components of the strain tensor $\boldsymbol{\epsilon}^{\boldsymbol{pd}}$ of a point defect are given by [5]

$$\epsilon_{ij}^{pd} = -\frac{3}{2}\frac{a^3\left((1+\beta)^{1/3}-1\right)}{r^3}\frac{r_i r_j}{r^2} \tag{18}$$

with $r_{i=1,2,3} = (x, y, z)$ respectively, $r = \sqrt{x^2+y^2+z^2}$ and a the lattice constant of iron. The mismatch parameter β is defined as the relative difference in volume between the distorted volume (V) and undistorted volume (V_0)

$$V = V_0(1+\beta) \tag{19}$$

An interstitial or foreign atom bigger than a lattice atom is described by a characteristic volume expansion, $\beta > 1$. A vacancy or foreign atom smaller than a lattice atom is described by a characteristic volume reduction , $\beta < 1$.
The stress components σ_{ij}^{pd} are calculated by the constitutive relation

$$\sigma_{ij}^{pd} = C_{ijkl}\epsilon_{kl}^{pd} \tag{20}$$

with $\mathbf{C}$ a material dependent positive-definite symmetric fourth-order tensor. The expressions (18) and (20) are isotropic, thus independent of lattice directions and can be used unchanged.

C. Dynamics

The evolution of the magnetic dipoles $\mathbf{m}$ is expressed in terms of the effective field by the Landau-Lifshitz-equation (LL-equation)

$$\frac{\partial \mathbf{m}}{\partial t} = \frac{\gamma_G}{1+\alpha^2}\mathbf{m}\times\mathbf{H}_{eff} - \frac{\alpha\gamma_G}{1+\alpha^2}\mathbf{m}\times(\mathbf{m}\times\mathbf{H}_{eff}) \tag{21}$$

with α and γ_G the damping constant and the gyromagnetic constant respectively. The static micromagnetic equilibrium condition, usually formulated as $\mathbf{m}\times\mathbf{H}_{eff} = 0$, follows directly from the LL-equation (21).

IV. 3D MICROMAGNETIC MODEL

In Fig 1 the micromagnetic model of the monocrystal is shown as a cuboid subdivided in $N_x \times N_y \times N_z$ cubes with sides Δ. The crystallographic axes x', y', z' are defined with respect to the xyz-coordinate system in terms of Euler angles (ϕ, θ, ψ) that define the rotation matrix $\mathbf{R}(\phi, \theta, \psi)$ which rotates the xyz-coordinate system towards the $x'y'z'$-coordinate system [7]. Each cell in the space discretization contains one single magnetization vector $\mathbf{m}$. The space derivatives appearing in (4) are approximated by a classical finite

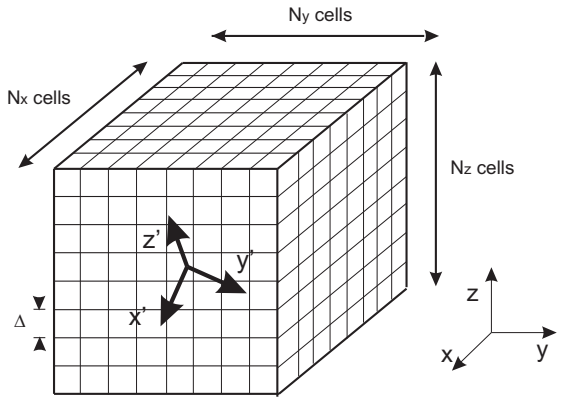

Fig. 1. Scheme of the micromagnetic model of a cuboid monocrystal

difference method. The magnetostatic field (7) together with the exchange field (4) is calculated by Fast Fourier Transforms in order to save computational time.

The initialization of the total stress is done by adding the stress contributions of the different defect structures, each according to there own orientation in the crystal as outlined above. Hereby, the intrinsic stress caused by magnetostriction is neglected so (total) strain compatibility

$$\nabla\times(\nabla\times\boldsymbol{\epsilon})^T = 0 \tag{22}$$

can not be guaranteed ($\boldsymbol{\epsilon}$ is the total strain tensor). This approximation is called the relaxed approach and is proven to be reasonable for thin materials with low magnetostriction [6].

For the time discretization the quasi-static applied field $\mathbf{H}_a$ is approximated with a piecewise constant time function. It is assumed that at the moment the applied field $\mathbf{H}_a$ jumps from a constant value to the next one, the material is in static micromagnetic equilibrium. Using the LL-equation (21), the magnetization dynamics in each basis cell is computed through time stepping until a new static micromagnetic equilibrium is obtained corresponding with the new constant value for the applied field $\mathbf{H}_a$. The magnetization dynamics is evaluated analytically at $[t_i, t_i+1]$ by introducing in each basis cell a local (u,v,w)-system with the u-axis parallel with $\mathbf{H}_{eff}(t_i)$. The LL-equation (21) can be solved analytically in this framework when $\mathbf{H}_{eff}(t)$ is kept constant during the time step

$$\mathbf{H}_{eff}(t) = H_{eff}(t_i)\mathbf{e}_u \quad t_i \le t \le t_{i+1} \tag{23}$$

During the time step $\mathbf{m}$ evolves from $\mathbf{m}(t_i) = u_i\mathbf{e}_u + v_i\mathbf{e}_v + w_i\mathbf{e}_w$ at $t = t_i$ to $\mathbf{m}(t_{i+1}) = u_{i+1}\mathbf{e}_u + v_{i+1}\mathbf{e}_v + w_{i+1}\mathbf{e}_w$ at $t = t_i + \Delta t$ with

$$u_{i+1} = \frac{e^{q\alpha\Delta t}(1+u_i) - e^{-q\alpha\Delta t}(1-u_i)}{e^{q\alpha\Delta t}(1+u_i) + e^{-q\alpha\Delta t}(1-u_i)} \tag{24}$$

$$v_{i+1} = 2\frac{v_i\cos(q\Delta t) - w_i\sin(q\Delta t)}{e^{q\alpha\Delta t}(1+u_i) + e^{-q\alpha\Delta t}(1-u_i)} \tag{25}$$

$$w_{i+1} = 2\frac{v_i\sin(q\Delta t) + w_i\cos(q\Delta t)}{e^{q\alpha\Delta t}(1+u_i) + e^{-q\alpha\Delta t}(1-u_i)} \tag{26}$$

with $q = \gamma_G H_{eff}(t_i)/(1+\alpha^2)$. In order to improve the rate of convergence, α is chosen to be 1.

TABLE I
MICROSCOPIC MATERIAL CONSTANTS FOR PURE IRON

quantity	value	unit
$\mu_0 M_s$	2.16	$[T]$
A	$1.5\,10^{-11}$	$[Jm^{-3}]$
K_1	$0.48\,10^{5}$	$[Jm^{-3}]$
K_2	$-0.50\,10^{5}$	$[Jm^{-3}]$
λ_{100}	$22\,10^{-6}$	[]
λ_{111}	$-21\,10^{-6}$	[]
a	$0.3\,10^{-10}$	$[m]$
C_{11}	$2.41\,10^{11}$	$[Pa]$
C_{44}	$1.12\,10^{11}$	$[Pa]$
C_{12}	$1.46\,10^{11}$	$[Pa]$
G	$82\,10^{9}$	$[Pa]$
ν	0.33	[]
γ_G	$-2.21\,10^{5}$	$[mA^{-1}s^{-1}]$

V. INFLUENCE OF MICROSTRUCTURE ON THE HYSTERESIS LOOP

To determine what mechanisms influence the shape of the hysteresis loop several numerical experiments were performed. Table I shows the material constants for pure iron, used in the experiments with C_{ijkl} in Voigt's notation [2]. A first series of experiments is performed on a cuboid monocrystal with dimensions $1.28\,\mu m \times 2.56\,\mu m \times 1.28\,\mu m$ divided in cubes with sides $10\,nm$. Two cases are distinguished.

In the first case the crystal has no defects while in the second case the crystal has five dislocations (edge and screw dislocations). For each case three hysteresis loops are simulated. A first one with the applied field $\mathbf{H}_a$ parallel with the y-axis and lattice axes parallel with the xyz-axes i.e. parallel with the edges of the cuboid (see Fig 1), a second one with the applied field $\mathbf{H}_a$ parallel to the space diagonal of the cuboid and the lattice axes parallel to the xyz-axes and a third one with the applied field $\mathbf{H}_a$ parallel to the space diagonal and the lattice axes parallel with the directions determined by the Euler angles ($\phi = \pi/5$, $\theta = \pi/5$, $\psi = \pi/5$). The results are shown in Fig 2. Fig 3 shows the microscopic configuration of the magnetization vectors in three edge plains of the cuboid for the remanent magnetization ($\mathbf{H}_a = 0$) of the hysteresis loop in solid line of Fig 2(a).

A second experiment is performed on a spherical monocrystal with a radius of $0.64\,\mu m$ divided in cubes with sides $10\,nm$, the applied field $\mathbf{H}_a$ is chosen parallel with a lattice axis. The result is shown in Fig 4. For both experiments, the applied magnetic field $\mathbf{H}_a$ is approximated by a piecewise constant function, considering 400 equidistant time intervals. The mean magnetization is calculated in the direction of the applied field.

Comparison between the hysteresis loop with solid line of Fig 2(a) and the hysteresis of Fig 4 proves that the shape of the ferromagnet influences the mean magnetization drastically. Comparison between the hysteresis loops for the cuboid monocrystal of Fig 2 learns that the direction of the applied field $\mathbf{H}_a$ with respect to the lattice axes and the edges of the cuboid influences the shape of the hysteresis loop. Comparison between the hysteresis loops of Fig 2(a) and Fig 2(b) learns that dislocations also have a large influence on the macroscopic magnetization. The configuration of the magnetization dipoles in Fig 3 shows some magnetization

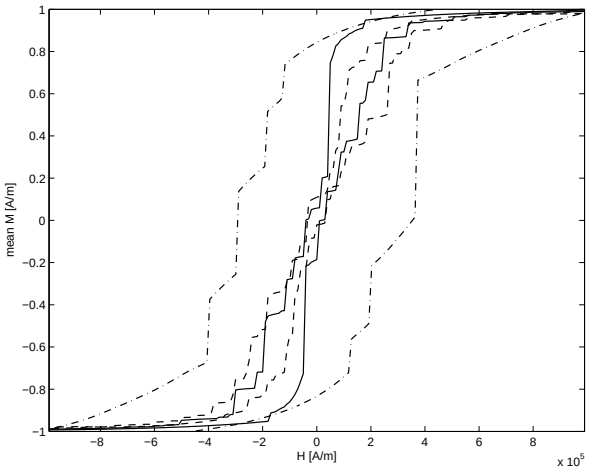

(a) zero dislocations

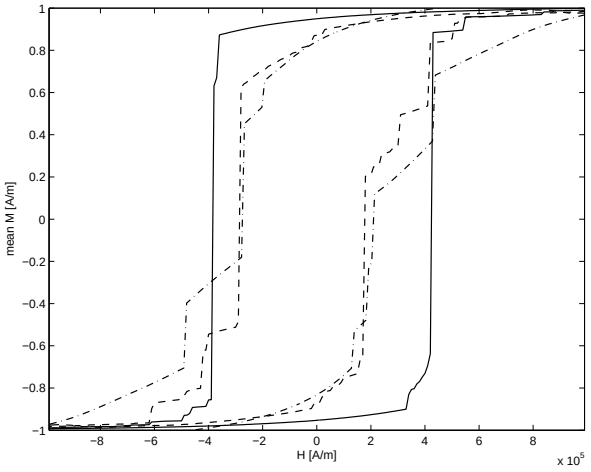

(b) five dislocations

Fig. 2. cuboid monocrystal with 0 and 5 dislocations, the solid line is the hysteresis loop for $\mathbf{H}_a$ parallel to the y-axis and lattice axes parallel to the xyz-axes, the dashed line for $\mathbf{H}_a$ parallel to a space diagonal and lattice axes parallel to the xyz-axes, the dash-dot line for $\mathbf{H}_a$ parallel to a space diagonal and lattice axes not parallel to the xyz-axes.

mechanics known in the literature [8]. In the $y = 0$ plain 90 degree domain walls come together in a vortex, the other plains are separated in two magnetic domains by a 180 degree domain wall.

VI. CONCLUSION

The presented micromagnetic proves that different mechanisms influence the macroscopic hysteresis loop of a monocrystal. First, the shape of the monocrystal has a large influence on the magnetization. Second, the directions of the applied field with respect to the lattice axes and geometrical axes are important. Third, lattice defects influence the shape of the hysteresis loop.

REFERENCES

[1] L. D. Landau and E. M. Lifshitz, *Electrodynamics of continiuous media*, Pergamom Press X: Oxford-London-New York-Paris, 1960.

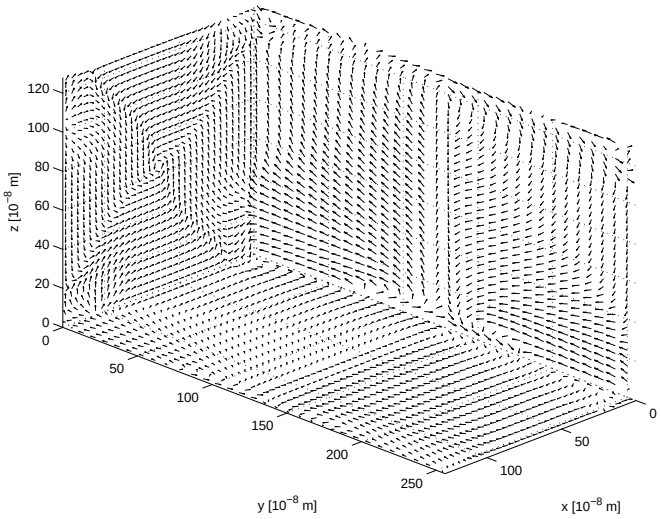

Fig. 3. Microscopic magnetization configuration for the hysteresis loop with solid line of Fig 2(a) with $\mathbf{H}_a = 0$ (remanent magnetization). The arrows show the magnetization in the three edge plains $x = 0$, $y = 0$ and $z = 0$

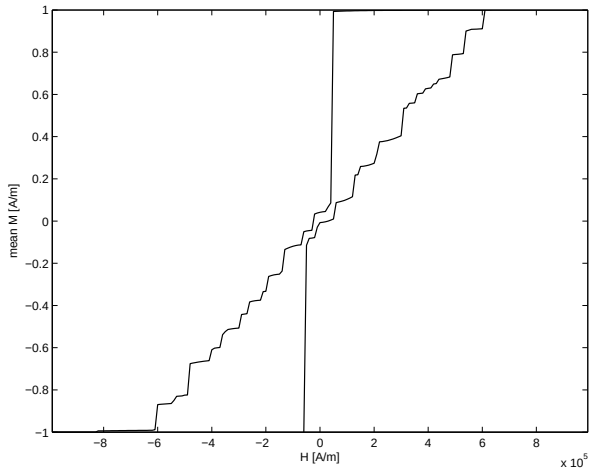

Fig. 4. Hysteresis loop for spherical monocrystal with zero dislocations for $\mathbf{H}_a$ parallel to a lattice axis

[2] H. Kronmüller and M. Fähnle, *Micromagnetism and the microstructure of ferromagnetic solids*, Cambridge University Press: Max-Planck-Institut für Metallfoschung, Stuttgart, Germany, 1994.
[3] F. R. N. Nabarro, "The mathematical Theory of Stationary Dislocations", *Advances in Physics*, Vol. 1(3), July 1952.
[4] G. E. Dieter, *Mechanical Metallurgy*, McGraw-Hill Book Company, London, 1988.
[5] D. T. Britton and M. Härting, "The Influence of Strain on Point Defect Dynamics", *Advanced Engineering Materials*, Vol. 4(8), 2002.
[6] Y. C. Shu, M. P. Lin and K. C. Wu, "Micromagnetic Modeling of magnetostrictive Materials under intrunsic Stress", *Mechanics of Materials*, Vol. 36, pp. 975-997, 2004.
[7] E. W. Weisstein, *Euler Angles*, From Mathworld–A Wolfram Web Resource. http://mathworld.wolfram.com/EulerAngles.html
[8] G. Bertotti, *Hysteresis in Magnetism*, Academic Press, 1994.

Proceedings

3rd IEEE Benelux YOUNG RESEARCHERS SYMPOSIUM in Electrical Power Engineering

27–28 April 2006, Ghent, Belgium

organized by

IEEE Joint IAS–PELS–PES Benelux Chapter

Electrical Energy Laboratory (EELAB), Ghent University

Editors: L. Dupré and L. Vandevelde

ISBN: 90-8106-481-9
Wettelijk Depot: D/2006/10.913/1


Proceedings 3rd IEEE Benelux
YOUNG RESEARCHERS SYMPOSIUM
in Electrical Power Engineering
ISBN: 90-8106-481-9
ALL RIGHTS RESERVED
Depot: D/2006/10.913/1
COMPACT disc DIGITAL DATA
UNIVERSITEIT GENT
IEEE
IAS/PELS/PES Benelux Chapter
April 27-28, 2006
Ghent, Belgium